

# Phonon renormalisation in doped bilayer graphene

A. Das<sup>1</sup>, B. Chakraborty<sup>1</sup>, S. Piscanec<sup>2</sup>, S. Pisana<sup>2</sup>, A. K. Sood<sup>1,\*</sup> and A. C. Ferrari<sup>2†</sup>  
<sup>1</sup>*Department of Physics, Indian Institute of Science, Bangalore 560012, India*  
<sup>2</sup>*Engineering Department, Cambridge University, Cambridge CB3 0FA, UK*

We report phonon renormalisation in bilayer graphene as a function of doping. The Raman G peak stiffens and sharpens for both electron and hole doping, as a result of the non-adiabatic Kohn anomaly at the  $\Gamma$  point. The bilayer has two conduction and valence subbands, with splitting dependent on the interlayer coupling. This results in a change of slope in the variation of G peak position with doping, which allows a direct measurement of the interlayer coupling strength.

PACS numbers: 73.63.-b, 63.20.Kr, 81.05.Uw, 78.30.Na,

Graphene is the latest carbon allotrope to be discovered [1, 2, 3, 4, 5]. Near-ballistic transport at room temperature and high carrier mobilities[2, 3, 4, 5, 6, 7, 8], make it a potential material for nanoelectronics [9, 10, 11], especially for high frequency applications. It is now possible to produce areas exceeding thousands of square microns by means of micro-mechanical cleavage of graphite. An ongoing effort is being devoted to large scale deposition and growth on different substrates of choice.

Unlike single layer graphene (SLG), where electrons disperse linearly as massless Dirac fermions[1, 2, 3, 4, 5], bilayer graphene (BLG) has two conduction and valence bands, separated by  $\gamma_1$ , the interlayer coupling[12, 13]. This was measured to be  $\sim 0.39\text{eV}$  by angle resolved photoelectron spectroscopy[14]. A gap between valence and conduction bands could be opened and tuned by an external electric field ( $\sim 100\text{meV}$  for  $\sim 10^{13}\text{cm}^{-2}$  doping)[15, 16], making BLG a tunable-gap semiconductor.

Graphene can be identified in terms of number and orientation of layers by means of elastic and inelastic light scattering, such as Raman[17] and Rayleigh spectroscopies[18, 19]. Raman spectroscopy also allows

monitoring of doping and defects[4, 20, 21, 22, 23, 24, 25]. Indeed, Raman spectroscopy is a fast and non-destructive characterization method for carbons[26]. They show common features in the  $800\text{-}2000\text{cm}^{-1}$  region: the G and D peaks, around  $1580$  and  $1350\text{cm}^{-1}$ , respectively. The G peak corresponds to the  $E_{2g}$  phonon at the Brillouin zone center ( $\Gamma$ ). The D peak is due to the breathing modes of  $\text{sp}^2$  atoms and requires a defect for its activation[27, 28, 29]. The most prominent feature in SLG is the second order of the D peak: the 2D peak[17]. This lies at  $\sim 2700\text{cm}^{-1}$  and involves phonons at  $\mathbf{K}+\Delta\mathbf{q}$ [17, 23].  $\Delta\mathbf{q}$  depends on the excitation energy, due to double-resonance, and the linear dispersion of the phonons around  $\mathbf{K}$ [17, 29, 30]. 2D is a single peak in SLG, whereas it splits in four in BLG, reflecting the evolution of the band structure[17]. The 2D peak is always seen, even when no D peak is present, since no defects are required for overtone activation.

In SLG, the effects of back and top gating on G-peak position ( $\text{Pos}(\text{G})$ ) and Full Width at Half Maximum ( $\text{FWHM}(\text{G})$ ) were reported in Refs[20, 21, 24].  $\text{Pos}(\text{G})$  increases and  $\text{FWHM}(\text{G})$  decreases for both electron and hole doping. The G peak stiffening is due to the non-adiabatic removal of the Kohn-anomaly at  $\Gamma$ [20, 31].  $\text{FWHM}(\text{G})$  sharpening is due to blockage of phonon decay into electron-hole pairs due to the Pauli exclusion principle, when the electron-hole gap is higher than the phonon energy[20, 32], and saturates for a Fermi shift bigger than half phonon energy[20, 21, 32]. A similar behavior is observed for the  $\text{LO-G}^-$  peak in metallic nanotubes[33], for the same reasons. The conceptually different BLG band structure is expected to renormalize the phonon response to doping differently from SLG[13, 34]. Here we prove this, by investigating the effect of doping on the BLG G and 2D peaks. The G peak of doped BLG was recently investigated[35], and reproduced that of SLG, due to the very low doping range ( $\sim 5 \times 10^{12}\text{cm}^{-2}$ ), not enough to cross the second BLG subband. Here we reach much higher values ( $\sim 5 \times 10^{13}\text{cm}^{-2}$ ), probing the further renormalisation resulting from crossing to the second BLG subband.

We recently demonstrated a SLG top-gated by poly-

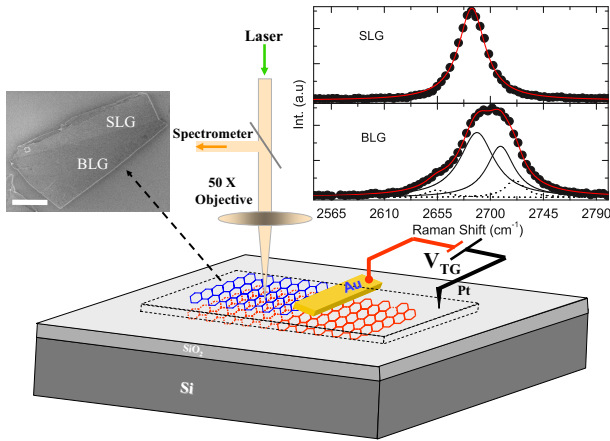


FIG. 1: (color online). Experimental setup. The black dotted box on  $\text{SiO}_2$  indicates the polymer electrolyte (PEO +  $\text{LiClO}_4$ ). The left inset shows an SEM image of the SLG and BLG. Scale bar:  $4\mu\text{m}$ . The right inset, the 2D Raman band

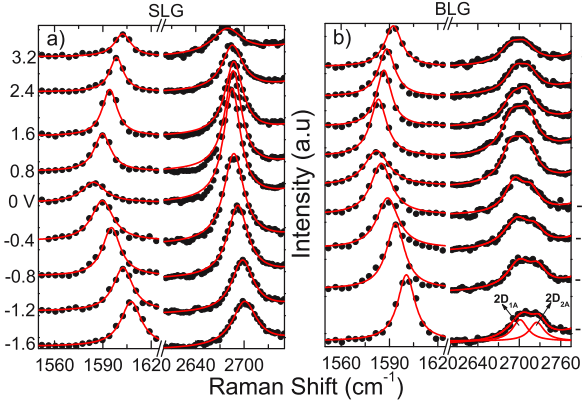


FIG. 2: (color online). Raman spectra of (a) SLG; (b) BLG at several  $V_{TG}$ . Red lines fits to the experimental data.

mer electrolyte[24], able to span a large doping range, up to  $\sim 5 \times 10^{13} \text{cm}^{-2}$ [24]. This is possible because the nanometer thick Debye layer[24, 36, 37] gives a much higher gate capacitance compared to the usual 300nm  $\text{SiO}_2$  back gate[5]. We apply here this approach to BLG. Fig.1 shows the scheme of our experiment. A sample is produced by micromechanical cleavage of graphite. This consists of a SLG extending to a BLG, as proven by the characteristic SLG and BLG 2D peaks in the inset of Fig.1[17]. An Au electrode is then deposited by photolithography covering both SLG and BLG, Fig.1. Top gating is achieved by using a solid polymer electrolyte consisting of  $\text{LiClO}_4$  and polyethylene oxide (PEO) in the ratio 0.12:1[24]. The gate voltage is applied by placing a platinum electrode in the polymer layer. Note that the particular shape of our sample, consisting of a BLG, with a protruding SLG, ensures the top gate to be effectively applied to both layers at the same time. This would not necessarily be the case for a monolithic BLG, where, due to screening effects, the gate would give a separate evolution of the Raman spectra of the top and bottom layers[38]. Measurements are done with a WITEC confocal (X50 objective) spectrometer with 600 lines/mm grating, 514.5 nm excitation, at  $< 1 \text{mW}$  to avoid heating. For a given top gate voltage,  $V_{TG}$ , spectra are recorded after 10 mins. Figs.2(a,b) plot the spectra as a function of  $V_{TG}$ . We use Voigt functions to fit the G peak in both SLG and BLG. The SLG 2D band is fitted to one Lorentzian. The BLG 2D band is fitted to four Lorentzians,  $2D_{1A}, 2D_{1B}, 2D_{2A}, 2D_{2B}$  [17], Fig.1. As previously discussed, two of these,  $2D_{1A}$  and  $2D_{2A}$ , are much stronger[17]. Thus, we focus on these.

To get a quantitative understanding, it is necessary to convert  $V_{TG}$  into a  $E_F$  shift. For electrolytic gating, the chemical potential is  $eV_{TG} = E_F^{SLG} + e\phi^{SLG} = E_F^{BLG} + e\phi^{BLG}$ . The electrostatic potential  $\phi = \frac{ne}{C_{TG}}$  is determined by the geometrical capacitance  $C_{TG}$  and carrier concentration  $n$  ( $e$  is the electron charge), while  $E_F/e$  by the chemical (quantum) capacitance of graphene. For

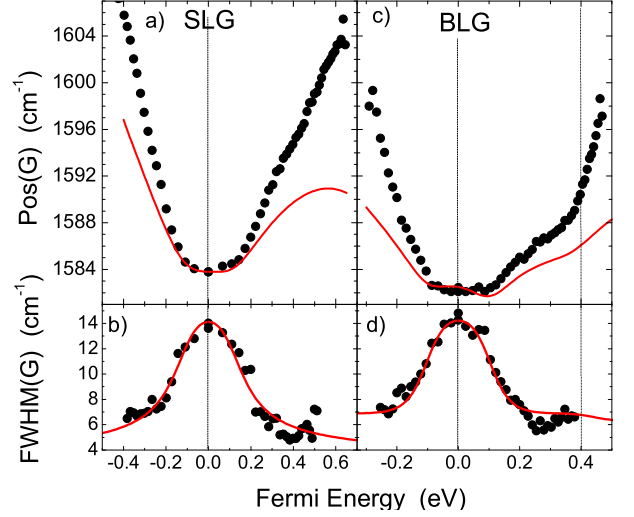


FIG. 3: (color online). Pos(G) for (a) SLG; (c) BLG as a function of Fermi energy. FWHM(G) of (b) SLG; (d) BLG as a function of Fermi energy. Solid lines: theoretical predictions.

SLG,  $n^{SLG} = \mu E_F^2$ , where  $\mu = \frac{g_s g_v}{4\pi\gamma^2} = \frac{1}{\pi(\hbar v_F)^2}$ ,  $g_s = g_v = 2$  are spin and valley degeneracies,  $\gamma = \frac{\sqrt{3}}{2}\gamma_0 a$ , with  $\gamma_0$  the nearest-neighbor tight binding parameter,  $a$  the graphene lattice parameter, and  $v_F$  is the Fermi velocity. Thus:

$$eV_{TG} = E_F + \nu E_F^2 \quad (1)$$

For BLG[13, 39, 40]  $n^{BLG} = \mu[\gamma_1 E_F + E_F^2]$  for  $E_F < \gamma_1$  and  $n^{BLG} = 2\mu E_F^2$  for  $E_F > \gamma_1$ . Thus:

$$eV_{TG} = (1 + \nu\gamma_1)E_F + \nu E_F^2, \quad E_F < \gamma_1 \quad (2)$$

$$= E_F + 2\nu E_F^2, \quad E_F > \gamma_1$$

where  $\nu = \frac{e^2}{\pi C_{TG}(\hbar v_F)^2}$ . We take  $C_{TG} = 2.2 \times 10^{-6} \text{Fcm}^{-2}$ [33], and  $\gamma_1 = 0.39 \text{eV}$  constant with doping (since its variation for  $n$  up to  $\sim 10^{13} \text{cm}^{-2}$  is  $< 5\%$ )[14, 15]). Eqs.1,2 then give  $E_F$  as a function of  $V_{TG}$ .

Fig.3 plots the resulting Pos(G), FWHM(G) as a function of  $E_F$ . In SLG, Pos(G) does not increase up to  $E_F \sim 0.1 \text{eV}$  ( $\sim \hbar\omega_0/2$ ), where  $\omega_0$  is the frequency of the  $E_{2g}$  phonon in the undoped case ( $\hbar\omega_0/(2\pi\hbar c) = \text{Pos}(G_0)$ , with  $c$  the speed of light), and then increases with  $E_F$ . Fig.3b,d indicate that in SLG and BLG, FWHM(G) decreases for both electron and hole doping, as expected since phonons decay into real electron-hole pairs when  $E_F < \hbar\omega_0/2$ [20]. Fig.3c plots Pos(G) of BLG. (i) Pos(G) does not increase until  $E_F \sim 0.1 \text{eV}$  ( $\sim \hbar\omega_0/2$ ). (ii) Between 0.1 and 0.4eV, the BLG slope  $R = \frac{d\text{Pos}(G)}{dE_F}$  is smaller than the SLG one. (iii) A kink is observed in Fig.3b at  $E_F \sim 0.4 \text{eV}$ . (iv) Beyond  $E_F > 0.4 \text{eV}$  the slope is larger than in SLG. (v) The kink position does not significantly depend on  $\gamma_1$  used to convert  $V_{TG}$  in  $E_F$  (e.g. a  $\sim 66\%$  change in  $\gamma_1$  modifies  $E_F$  by  $\sim 6\%$ ).

These trends can be explained by considering the effects doping on the phonons: (i) a change of the equilib-

rium lattice parameter with a consequent “static” stiffening/softening,  $\Delta Pos(G)^{st}$ ; (ii) the onset of “dynamic” effects beyond the adiabatic Born-Oppenheimer approximation, that modify the phonon dispersion close to the Kohn anomalies,  $\Delta Pos(G)^{dyn}$ [20, 31]. Thus, the total phonon renormalization can be written as[20, 31]:

$$Pos(G_{E_F}) - Pos(G_0) = \Delta Pos(G) = \Delta Pos(G)^{st} + \Delta Pos(G)^{dyn} \quad (3)$$

For SLG, we compute  $\Delta Pos(G)^{st}$  by converting  $E_F$  into the corresponding electron density  $n^{SLG}$ , then using Eq.3 of Ref.[31]. For BLG, we assume  $n^{BLG}$  equally distributed on the two layers, each behaving as a SLG with an electron concentration  $n^{BLG}/2$ . Eq.3 of Ref.[31] is then used to compute  $\Delta Pos(G)^{st}$  for BLG.  $\Delta Pos(G)^{dyn}$  is calculated from the phonon self-energy  $\Pi$ [41]:

$$\hbar \Delta Pos(G)^{dyn} = \text{Re}[\Pi(E_F) - \Pi(E_F = 0)]. \quad (4)$$

The electron-phonon coupling (EPC) contribution to FWHM(G) is given by[41, 42, 43]:

$$\text{FWHM(G)}^{EPC} = 2\text{Im}[\Pi(E_F)] \quad (5)$$

The self-energy for the  $E_{2g}$  mode at  $\Gamma$  in SLG is[20, 31]:

$$\Pi(E_F)^{SLG} = \alpha' \int_{-\infty}^{\infty} \frac{f(\epsilon) - f(-\epsilon)}{2\epsilon + \hbar\omega_0 + i\delta} |\epsilon| d\epsilon, \quad (6)$$

while for BLG it is given by [13]:

$$\begin{aligned} \Pi(E_F)^{BLG} &= \alpha' \int_0^{\infty} \gamma^2 k dk \sum_{s,s'} \sum_{j,j'} \phi_{jj'}^+ \\ &\times \frac{[f(\epsilon_{sjk}) - f(\epsilon_{s'j'k})][\epsilon_{sjk} - \epsilon_{s'j'k}]}{(\epsilon_{sjk} - \epsilon_{s'j'k})^2 - (\hbar\omega_0 + i\delta)^2} \end{aligned} \quad (7)$$

where  $\alpha' = \frac{\hbar A_{uc} EPC(\Gamma)^2}{\pi M \omega_0 (\hbar v_F)^2}$ ,  $A_{uc} = 5.24 \text{ \AA}^2$  is the graphene unit-cell area,  $M$  is the carbon atom mass,  $f(\epsilon) = 1/[\exp(\frac{\epsilon - E_F}{k_B T}) + 1]$  is the Fermi-Dirac distribution,  $\delta$  is a broadening factor accounting for charge inhomogeneity,  $EPC(\Gamma)$  is the electron phonon coupling[46].  $s = \pm 1$  and  $s' = \pm 1$  label the conduction (+1) and valence (-1) bands, while  $j = 1, 2$  and  $j' = 1, 2$  label the two parabolic subbands.  $\epsilon_{sjk}$  is computed from Eq.2.8 of Ref.[13], and  $\phi_{jj'}^+$  is given by Eq.3.1 of Ref.[13]. By using Eqs.6,7 in Eqs.4,5, we get  $\Delta Pos(G)^{dyn}$ ,  $\text{FWHM(G)}^{EPC}$  for SLG and BLG.

To compare Eqs.3,5 with the experimental data, we use  $\alpha' = 4.4 \times 10^{-3}$  (obtained from the DFT values of  $EPC(\Gamma)$  and  $v_F$ [20, 30]), the experimental  $\hbar\omega_0$  for SLG and BLG, and  $T=300\text{K}$ .  $\delta$  is fitted from the experimental  $\text{FWHM(G)}$  to  $\text{FWHM(G)} = \text{FWHM(G)}^{EPC} + \text{FWHM(G)}^0$ , with  $\text{FWHM(G)}^0$  a constant accounting for non-EPC effects (e.g. resolution and anharmonicity). For SLG (BLG) we get  $\delta = 0.13\text{eV}$  (0.03eV) and  $\text{FWHM(G)}^0 = 4.3\text{cm}^{-1}$  (5.1 $\text{cm}^{-1}$ ). These  $\delta$  values are then used to compute  $Pos(G)$ . Note that the relation between  $n$  and  $E_F$

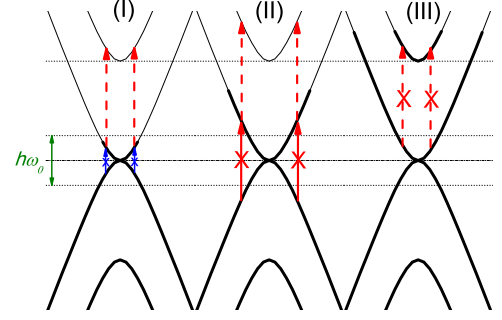


FIG. 4: (color online). Phonon renormalization for BLG: (I)  $E_F < \hbar\omega_0$ , (II)  $\hbar\omega_0 < E_F < \gamma_1$ , (III)  $E_F > \gamma_1$ . Blue and red arrows correspond respectively to positive and negative contributions to  $\Pi$ . Solid and dashed arrows correspond to interband and intraband processes respectively.

implies that charge inhomogeneity causes different  $E_F$  broadening in SLG and BLG (e.g.  $\delta n \sim 10^{12} \text{cm}^{-2}$  would give 0.13eV and 0.03eV in SLG and BLG, respectively).

The solid lines in Fig. 3 are the theoretical  $Pos(G)$  and  $\text{FWHM(G)}$  trends. The experimental and theoretical  $\text{FWHM(G)}$  are in excellent agreement, as expected since the latter was fitted to the former. The theoretical  $Pos(G)$  captures the main experimental features. In particular, the flat dependence for  $|E_F| < 0.1 \text{ eV}$  in both SLG and BLG, and the kink at  $\sim 0.4 \text{ eV}$  in BLG. This kink is the most striking difference between SLG and BLG. It is the signature of the second subband filling in BLG. Indeed, a shift of  $E_F$ , by acting on  $f(\epsilon)$  in Eq.7, modifies the type and number of transitions contributing to  $\Pi$ . The only transitions giving a positive contribution to  $\Pi$  are those for which  $|\epsilon_{s,j,k} - \epsilon_{s',j',k}| < \hbar\omega_0$ , i.e. a subset of those between  $(s = -1; j = 1)$  and  $(s = 1; j = 1)$  (interband transitions, solid blue lines in Fig. 4). Interband transitions with  $|\epsilon_{s,j,k} - \epsilon_{s',j',k}| > \hbar\omega_0$  (solid red lines in Fig. 4) and all intraband (between  $(s = \pm 1; j = 1)$  and  $(s = \pm 1, j = 2)$ , dashed red lines in Fig. 4) contribute to  $\Pi$  as negative terms. It is convenient to distinguish three different cases: (I),  $|E_F| < \hbar\omega_0$ , (II)  $\hbar\omega_0 < |E_F| < \gamma_1$ , and (III)  $|E_F| > \gamma_1$ . For simplicity let us assume  $E_F > 0$  (the same applies for  $E_F < 0$ ). In case (I), positive contributions from interband transitions are suppressed, and new negative intraband transitions are created. This results in strong phonon softening at low temperatures[35]. At  $T=300\text{K}$ , these effects are blurred by the fractionary occupation of the electronic states, resulting in an almost doping independent phonon energy (see Fig.3b). In case (II), a shift of  $E_F$  suppresses negative interband contributions and creates new negative intraband transitions. By counting their number and relative weight (given by  $\Phi_{jj'}/(\epsilon_{s,j,k} - \epsilon_{s',j',k})$ ), one can show that interband transitions outweigh intraband ones, resulting in phonon hardening. Case (III) is similar to (II), with the difference that the second subband filling suppresses negative intraband transitions at  $\mathbf{k} \sim \mathbf{K}$ ,

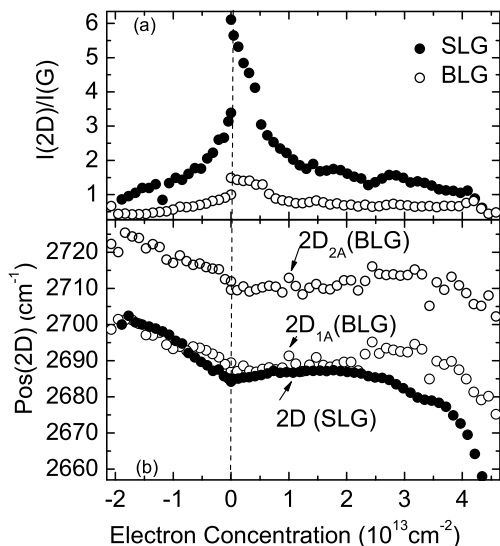


FIG. 5: (a) Ratio of 2D and G peaks intensities for SLG (solid circles) and BLG (open circles) as a function of  $n$ . (b) Position of 2D for SLG (solid circles) and 2D main components for BLG (open circles) as a function of  $n$ .

further enhancing the phonon hardening. It is also possible to demonstrate that, for  $T$  and  $\delta \rightarrow 0$ , the slope of  $\Delta \text{Pos}(G)^{\text{dyn}}$  just above  $E_F = \gamma_1$  is double than that just below. Thus, the kink in Fig.3 is a direct measurement of the interlayer coupling strength from Raman spectroscopy.

In SLG the intensity ratio of 2D and G,  $I(2D)/I(G)$ , has a strong dependence on doping[24]. Fig.5a plots  $I(2D)/I(G)$  as a function of doping. For BLG we take the highest amongst  $2D_{1A}$  and  $2D_{2A}$ . The SLG dependence reproduces our previous results[24]. However, we find an almost constant ratio in BLG. Fig.5b plots the doping dependence of  $\text{Pos}(2D)$  in SLG, and  $\text{Pos}(2D_{1A})$ ,  $\text{Pos}(2D_{2A})$  in BLG. To a first approximation, this is governed by lattice relaxation, which explains the overall stiffening for hole doping and softening for electron doping[24]. A quantitative understanding is yet to emerge, and beyond DFT many body effects need be considered.

To conclude, we have simultaneously measured the behavior of optical phonons in single and bilayer graphene as a function of doping. In the latter, the G peak renormalizes as the Fermi energy moves from the 1st to the 2nd subband, allowing a direct measurement of  $\gamma_1 \sim 0.4\text{eV}$ .

We thank D. Basko for useful and stimulating discussions. AKS acknowledges funding from the Department of Science and Technology, India, SP from Pembroke College and the Maudslay society, ACF from The Royal Society and The Leverhulme Trust.

\* Electronic address: asood@physics.iisc.ernet.in

† Electronic address: acf26@eng.cam.ac.uk

- [1] K.S. Novoselov et al. Science **306**, 666 (2004)
- [2] K.S. Novoselov, et al. Nature **438**,197 (2005).
- [3] Y. Zhang et al. Nature, **438**, 201 (2005).
- [4] J. C. Charlier et al. Topics Appl. Phys. **111**, 673 (2008)
- [5] A. K. Geim, K. S. Novoselov; Nat. Mater., **6**, 183 (2007).
- [6] S. V. Morozov et al. Phys. Rev. Lett., **100** 016602 (2008).
- [7] X. Du et al. cond mat. arXiv:0802.2933
- [8] K. I. Bolotin et al arXiv:0802.2389; arXiv:0805.1830
- [9] M. C. Lemme et al. IEEE El. Dev. Lett. **28**, 282 (2007).
- [10] M. Y. Han et al. Phys. Rev. Lett. **98**, 206805 (2007).
- [11] Z. Chen et al. Physica E, **40**, 228 (2007).
- [12] E.McCann,V.I.Falko, Phys. Rev. Lett.,**96** 086805 (2006)
- [13] T. Ando, J. Phys. Soc. Jpn. **76**, 104711 (2007).
- [14] T. Ohta et al. Science **313**, 951 (2007).
- [15] E. McCann, Phys. Rev. B **74**, 161403 (R) (2006).
- [16] E. V. Castro et al. Phys. Rev. Lett. **99**, 216802 (2007).
- [17] A. C. Ferrari et al. Phys. Rev. Lett. **97**, 187401 (2006).
- [18] C. Casiraghi et al. Nano. Lett. **7**, 2711 (2007).
- [19] P. Blake et al. Appl. Phys. Lett. **91**, 063124 (2007).
- [20] S. Pisana et al., Nature Mat. **6**,198 (2007).
- [21] J. Yan et al. Phys.Rev.Lett. **98**, 166802 (2007).
- [22] C. Casiraghi et al. Appl. Phys. Lett. **91**, 233108 (2007)
- [23] A. C. Ferrari, Solid State Comm. **143**, 47 (2007).
- [24] A. Das et al., Nature Nanotech. **3**, 210 (2008).
- [25] A. Das et al., cond-mat/0710.4160 (2007).
- [26] A. C. Ferrari, J. Robertson (eds), Raman spectroscopy in carbons: from nanotubes to diamond, Theme Issue, Phil. Trans. Roy. Soc. A **362**, 2267-2565 (2004).
- [27] F.Tuinstra,J.L. Koenig, J. Chem. Phys.**53**, 1126 (1970).
- [28] A.C. Ferrari, J. Robertson Phys. Rev. B **61**, 14095 (2000); *ibid.* 64, 075414 (2001).
- [29] C. Thomsen, S. Reich, Phys. Rev.Lett. **85**, 5214 (2000).
- [30] S. Piscanec et al. Phys. Rev. Lett. **93**, 185503 (2004).
- [31] M. Lazzeri, F. Mauri, Phys. Rev. Lett. **97**, 266407 (2006).
- [32] M. Lazzeri et al. Phys. Rev. B **73**, 155426 (2006).
- [33] A. Das et al. Phys Rev Lett. **99**, 136803 (2007).
- [34] T. Ando, J. Phys. Soc. Jpn. **75**, 124701 (2006).
- [35] J. Yan et al. cond-mat/0712.3879v1 (2007).
- [36] K. T. Nguyen, Phys. Rev. Lett. **98**, 145504 (2007).
- [37] C. Lu et al. Nano Lett. **4**, 623 (2004).
- [38] A. Das, A. C. Ferrari, A. K. Sood, unpublished (2008)
- [39] Note that in Fig.3 of Ref.[13] both SLG density of states and electron concentration are multiplied by a factor 2.
- [40] A. H. Castro Neto et al. cond-mat/0709.1163v1 (2007).
- [41] W.E.Pickett,P.B.Allen, Phys. Rev. B**16**, 3127 (1977).
- [42] P. B. Allen, Phys. Rev. B **6**, 2577 (1972).
- [43] Note that the phonon self-energy imaginary part corresponds to G half width at half maximum,  $\text{HWHM}(G)$ , as for Eq.8 in Ref.[42]. Thus, the factor 2 to compute  $\text{FWHM}(G)$  in Eq.5. This is sometimes neglected in literature. For example,  $\Delta\Gamma$  in Eq.1 of Ref.[21] represents  $\text{HWHM}(G)$ , and not  $\text{FWHM}(G)$ . Ref.[21] then compares this with  $\text{FWHM}(G)$  calculated in Eq.3 of Ref.[32], finding  $D^2/4 = \langle D_F^2 \rangle_F$ . However, the correct relation should be  $D^2/2 = \langle D_F^2 \rangle_F$ . Because of this, the coupling constant of Ref.[21] is  $\lambda = 2\alpha'$  instead of  $\lambda = \alpha'$ . Similarly, "broadening" in Figs.4,6 of Ref.[13] and Fig.4 of Ref.[34] is  $\text{HWHM}(G)$ , not  $\text{FWHM}(G)$ . Also, Fig.6 in Ref.[44] mistakenly compares the experimental  $\text{FWHM}$  of the  $G^-$

peak of metallic SWNTs with the theoretical HWHM.

[44] K.Ishikawa,T.Ando, J.Phys.Soc.Jap.**75**, 084713 (2006).

[45] Note that the prefactor of Eq.7 of Ref.[20] should be  $\frac{\omega_0 \alpha'}{4c}$

[46] EPC( $\Gamma$ ) is equivalent to  $\langle G_{\Gamma}^2 \rangle_F$  as defined in Ref.[32]